Proceedings of ASME Turbo Expo 2020
Turbomachinery Technical Conference and Exposition
GT2020
June 22-26, 2020, London, England

GT2020-15047

INVESTIGATION OF ATOMIZATION BEHAVIORS OF LIQUID MONOPROPELLANTS IN PINTLE INJECTORS

Jacob Gamertsfelder[1], Prashant Khare[1*], and Luis Bravo[2]

[1]Department of Aerospace Engineering, University of Cincinnati, Cincinnati, OH 45221-0070
[2]Vehicle Technology Directorate, Army Research Laboratory, Aberdeen Proving Ground, MD 21005
*Email for correspondence: Prashant.Khare@uc.edu

ABSTRACT

This research effort focuses on the atomization physics of liquid monopropellents emanating from a pintle-type injector at high-pressure conditions. These injectors are used extensively in liquid-fueled propulsion systems, such as rockets and diesel engines, and undersea vehicles and munitions. While extensive research has been conducted in the past on bipropellant fuel injection and atomization, limited literature exists on the understanding of atomization processes of monopropellant fuels in a pintle injector configuration for viscous fluids at elevated pressures. Therefore, in the current work, injection and subsequent atomization processes of a liquid monopropellant fuel are investigated as it is injected through a pintle injector in a stagnant environment using direct numerical simulations. The pintle injector consists of an annulus with an outer diameter twice the size of the inner diameter, and center pintle that throttles the fuel out of the injector. The theoretical and mathematical formulation to investigate these two-phase problems is based on the three-dimensional incompressible Navier-Stokes equations with surface tension. A critical issue is the treatment of multi-scale liquid-liquid and gas-liquid interfaces, therefore, a state-of-the-art, high resolution, volume-of-fluid (VOF) interface capturing method is adopted to resolve the interfacial evolution. Surface tension is accommodated as a Dirac delta distribution function on the interface. The theoretical formulation outlined above is solved numerically using a finite volume method augmented by an adaptive mesh refinement (AMR) technique, based on an octree spatial discretization to improve the solution accuracy and efficiency. As a first step, for model validation, we simulate water injection in the aforementioned geometry at a flowrate of 44.4 g/s in a stagnant chamber at 1 atm and room temperature conditions. Comparison of our results with experimentally measured sauter mean diameter and spray angle shows excellent agreement – both quantities are within 4.2% of the measured quantities. Next, Otto fuel II injection and atomization are studied to elucidate the atomization characteristics of the fuel in a pintle injector. The dynamic viscosity of the representative liquid monopropellant, Otto fuel II is 0.0044 Pa-s, density is 1232 kg/m^3, and the surface tension at the gas-liquid interface is 0.03445 N/m. The operating conditions consist of p = 106.2 bar, T = 300 K, and inlet velocity u = 3.34 m/s, corresponding to a density ratio of 10, dynamic viscosity ratio of 212 and Weber number of 20 (based on gas density). Results indicate that a radially growing hollow cone spray film attached at the injector exit is formed. Instability waves are formed on the outer and inner surfaces of the cone that facilitates breakup. Once droplets are completely separated from the cone, they are convected to recirculation zones, thus interacting with the hollow cone and amplifying the instability waves to cause further breakup. Droplet size distributions and their time evolution are also calculated during the research effort to quantitatively characterize the atomization behaviors.

Keywords: pintle injector, atomization, monopropellants, volume of fluid, adaptive mesh refinement

NOMENCLATURE

σ	surface tension
κ	curvature
$\mathbf{n}$	vector normal to the fluid interface
δ_s	Dirac delta function
ρ_L	liquid density
ρ_g	gas density
μ_L	liquid viscosity
μ_g	gas viscosity
α	liquid fraction
d	annulus diameter
w	pintle width
c	clearance
We	Weber number
$\boldsymbol{u}$	velocity vector

INTRODUCTION

The ability to accurately predict multi-phase, multi-scale, multi-physics processes in combustion systems, including gas-turbine, diesel, torpedo and rocket engines is critical to the development of future propulsion systems. Spray atomization characteristics are especially important for combustors using monopropellant fuels because the system performance is conditioned by the propellant droplet size distributions, and is the rate-controlling process [1, 2]. Evaporation of monopropellant and the ensuing combustion are accelerated if the droplet size is smaller, so any atomization process leading to a reduction in drop size is of prime importance in combustor design. Many injectors, such as swirling, pintle, jet impingement, and air-blast atomization are used for this purpose in contemporary liquid-fueled combustion devices. Among these, pintle injectors, also known as variable area injectors have been widely used in diesel, rocket and torpedo engines, most famous among which is the Apollo Lunar Module Descent Engine [3], because of their enhanced throttling ability and design simplicity [4].

Figure 1 shows a schematic diagram of a centrally located single element pintle injector for monopropellant engines. It consists of an annulus through which the fuel is injected radially into the chamber. In bi-propellant pintle injectors, the oxidizer is often injected through the annulus and the fuel is injected coaxially such that it impinges on the radially emanating oxidizer stream [3, 4]. By moving the pintle thrust can be modulated; the maximum thrust being achieved when the injection orifice is fully open (as shown in Figure 1). As the pintle moves away from the chamber (towards left in Figure 1), the injection area reduces leading to lower thrust. Reduction in the injection area leads to higher injection velocities, leading to good atomization and ensuing combustion characteristics even at lower thrust conditions.

Although tremendous progress has been made in the last decade to model multiphase flows relevant to pintle injector based configurations [5-7], especially for bi-propellant pintle injectors, prediction, and control of spray statistics in realistic chemically reacting configurations (e.g., relevant pressures, Weber and Reynolds numbers) remains an outstanding challenge, not only in industrial/military applications but even in fundamental scientific endeavors. Concerning monopropellant spray and atomization processes using pintle-injectors, to the best of our knowledge, no comprehensive theories or computational models have been established to analyze and optimize the spray behaviors at relevant design and off-design operating conditions. This situation is further exasperated when the monopropellant fuel is highly viscous; for such fuels, no study in the past has addressed the detailed multiphase flowfield and the associated atomization characteristics at chamber operating conditions, especially for low thrust injection conditions. One of the major challenges arises from the widely disparate length and time scales, and the associated difficulties in resolving local interfacial phenomena (e.g., instabilities, and pinch-off) that dictate the global behaviors. Much of the existing understanding and many of the design tools for liquid fuel injection, atomization and spray for pintle injector based monopropellants engines are, thus, empirically based and established through time-consuming and costly processes of trial and error. There is, therefore, an urgent need to enhance the fundamental understanding of liquid atomization process and subsequent spray behaviors, and develop predictive models that can be used for efficient design and control of characteristics, such as droplet sizes for monopropellant propulsion engines. Fortunately, recent advances in hardware technologies and numerical methodologies capable of accurately resolving liquid/gas interfaces [8-13] have made it possible to investigate the detailed spray and flow dynamic phenomena, such as those exhibited in monopropellant pintle injectors, with realistic turnaround times. Therefore, in this research effort, we address the atomization characteristics of a viscous (4.63 times that of water) monopropellant, Otto Fuel II [14, 15] at engine relevant pressures to establish the fundamental physics underlying the atomization and spray behaviors when the orifice is fully open using a volume of fluid based direct numerical simulation methodology developed by Pópinet [13].

The rest of the manuscript is organized into four sections. The next section details the technical approach, its rationale, and the theoretical formulation and numerical techniques used in this research. This is followed by model validation that is conducted by simulating the experiment conducted by Petrescu, et al. [16] and comparing the spray angle and droplet statistics with measurements. This is followed by results and discussion of the physical mechanisms governing the atomization of Otto Fuel II and the associated droplet statistics.

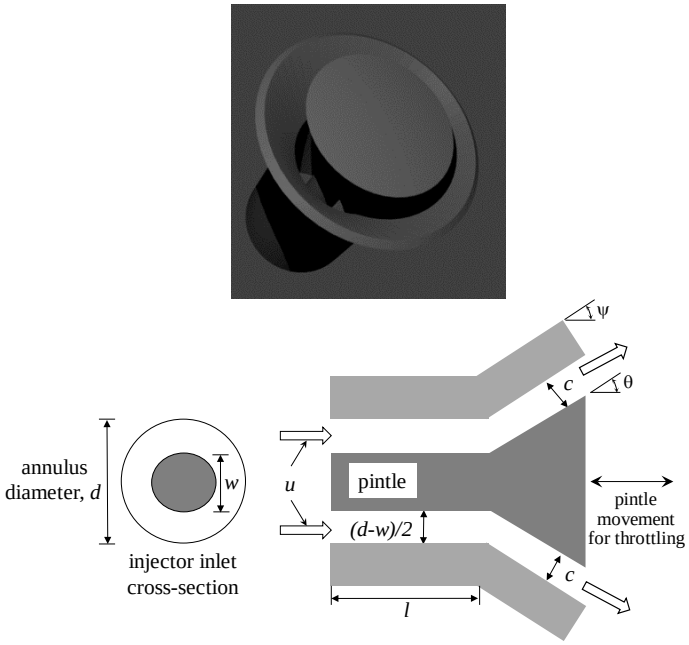

Figure 1. (a) 3D perspective view of the pintle injector used in this study. (b) Schematic of the cross-section of the injector geometry with annulus diameter *d*, pintle width *w*, clearance *c*, and nozzle length *l*. Monopropellant fuel enters the annulus with a velocity, *u*.

TECHNICAL APPROACH

The current research poses two stringent challenges that need to be addressed to quantitatively identify the underlying physical processes present when a monopropellant fuel is injected through a pintle valve in the combustion chamber. The major processes are: (1) the presence of multiple phases and frequent interfacial topology changes, and (2) the existence of widely disparate length and time scales that need to be resolved in an accurate and computationally efficient manner. To accurately address the first issue, the most appropriate approach to investigate the flow physics of interest with high-fidelity is based on Eulerian-Eulerian framework, that is, all relevant phases (liquid and gaseous) being treated as continuous, and the interface between them is captured. This approach is also called the one-fluid approach in the literature [13]. To appropriately resolve the wide range of spatial and temporal scales, adaptive mesh refinement is adopted such that high-resolution is achieved in reasonable turnaround time. In addition, to isolate the hydrodynamic mechanisms, all numerical simulations will be conducted at non-vaporizing temperature conditions. Based on this rationale, the next subsection details the theoretical framework and numerical methods that are used in this research effort.

Theoretical Framework and Numerical Methodology

The proposed research will build on an established Navier Stokes Equation (NSE) solver that handles multiphase fluid dynamics, and multi-component fuel properties using high-fidelity numerical simulations. The theoretical and mathematical formulation of this multiphase, multi-fluid problem is based on a complete set of three-dimensional, incompressible, variable- density and viscosity conservation equations with surface tension in a Eulerian reference frame [13, 17]. A critical issue is the treatment of multi-scale liquid-liquid and gas-liquid interfaces with mass and momentum transport (vaporization and combustion are not considered to isolate hydrodynamics). To address this, a state-of-the-art, high resolution, volume-of-fluid (VOF) interface capturing method is adopted and implemented to track the large-scale interfacial evolution. Surface tension is modeled as a Dirac distribution function on the interface. The conservation of mass and momentum can thus be written as:

$$\frac{\partial \rho}{\partial t} + \nabla.(\rho \vec{u}) = 0 \tag{1}$$

$$\rho\left(\frac{\partial \vec{u}}{\partial t} + \vec{u}.\nabla\vec{u}\right) = -\nabla p + \nabla.(2\mu\overline{\overline{D}}) + \sigma\kappa\delta_s\vec{n} \tag{2}$$

where $\vec{u} = (u, v, w)$ is the fluid velocity, $\rho = \rho(\vec{x}, t)$ the density, $\mu = \mu(\vec{x}, t)$ the dynamic viscosity, and $\overline{\overline{D}}$ is the deformation tensor defined as $D_{ij} = 1/2(\partial u_i / \partial x_j + \partial u_j / \partial x_i)$. σ is the surface tension coefficient, κ and $\vec{n}$ are the radius of curvature and the unit vector normal to the interface, respectively. The Dirac delta distribution function, δ_s expresses the fact that the surface tension term is concentrated on the interface. To capture the multi-fluid interface, a variable $\alpha = \alpha(\vec{x}, t)$ is introduced, defined as the volume fraction of one of the fluids (liquid in this case) in a given computational cell. The density and viscosity in each finite volume are then defined as linear functions of α:

$$\rho(\alpha) = \alpha\rho_L + (1-\alpha)\rho_g \tag{3}$$

$$\mu(\alpha) = \alpha\mu_L + (1-\alpha)\mu_g \tag{4}$$

Subscripts *L* and *g* denote the liquid and the gas, respectively. Using equation 1, the advection equation for the density can be written as an equivalent equation for the volume fraction, given by:

$$\frac{\partial \alpha}{\partial t} + \nabla.(\alpha\vec{u}) = 0 \tag{5}$$

The resulting system of partial differential equations provides an accurate capability for modeling highly dynamic multiphase flow processes such as pintle injector primary breakup.

The governing equations described above are solved using a projection method based on variable density fractional step numerical methodology using Gerris framework developed by Pópinet [13]. The interim velocity is computed in the first step. The pressure field is then computed by solving the Poisson equation and projecting the interim velocity onto a divergence-free velocity field. Quad/octree spatial discretization is used in combination with a multigrid V-cycle Poisson solver to obtain the pressure distribution. The primitive variables -- momentum components, pressure, and volume fraction, are volume averaged and collocated at the cell centers of the discretized volume. This collocated definition of primitive variables is useful for mesh adaptation and facilitates the implementation of the Gudunov scheme for the non-linear convective terms. To treat the viscous terms accurately, an approximate projection method developed by Almgren, et al. [18] is used. The scalar VOF variable *f*, is obtained by solving the advection equation for the volume fraction. A piecewise-linear geometrical VOF scheme [19] generalized for quad/octree spatial discretization is used to solve equation 5. The value of α in each cell then corresponds to the fraction of the finite volumes filled with different phases. Computational cells completely filled with fluid 1 are characterized by α = 0 and fluid 2 by α = 1, and cells containing the interface are characterized by $0 < \alpha < 1$. Since face-centered velocities are divergence-free, and the function α is then advected using the computed velocity field. Details of the various numerical algorithms used in this paper can be found elsewhere [13, 20-22].

Even though fixed mesh algorithms have been used successfully for dynamically evolving interfacial flows, it is extremely computationally expensive and often cost prohibitive. AMR is one of the most efficient ways to mitigate this problem. The AMR implementation used in the present research is based on structured grids to facilitate the implementation of the various

numerical algorithms and reduce the computational overhead while providing excellent mass conservation characteristics. The octree discretization further assists in the implementation of the multigrid V-cycle solver for the solution of the Poisson equation. Structured adaptive mesh refinement (SAMR) grid methods have been successfully used by researchers to explore a wide range of physical phenomena, ranging from large scale numerical relativity, to cosmology and astrophysics [23-25] , fluid dynamics, and combustion simulations [26-29].

Therefore, to ensure that the wide range of spatial and temporal scales are resolved with high-fidelity, an adaptive mesh refinement (AMR) technique is implemented to improve the solution accuracy and efficiency. The adaptive quad/octree spatial discretization is especially useful for the liquid-gas and liquid-liquid interface refinement. The grid adaptation criterion depends on the physics under consideration. Several refinement criteria, including value-, gradient- and thickness-based are implemented to resolve the interfacial and interior characteristics of the liquid monopropellant as it is injected in an inert chamber. The grid is refined or coarsened by comparing the refinement indicator in each cell to a predefined threshold value. Further, the code is parallelized based on MPI libraries for massively parallel computations. Figure 2 shows an example of AMR that is used in this research effort. This framework has been used extensively for a wide range of multiphase flow problems, including liquid jet atomization in the presence of broadband inlet fluctuations, impinging liquid jets, droplet breakup and collision phenomena [30-35].

Various numerical schemes used for the spatial discretization impose restrictions on the maximum allowable time step that can be used to ensure numerical stability. These constraints are determined by the convective, viscous and surface tension terms and the time step is calculated based on the following criteria:

1. Convective term: this constraint is probably the most well-known and is defined by the CFL condition given by:

$$\max\left[\frac{|\mathbf{u}_{i,j,k}|\,\Delta t_{convection}}{\Delta}\right] < CFL_{\max} \tag{6}$$

This restriction ensures that the fluid volume convected to the neighboring cell is not more than the amount of fluid in the cell. We used a conservative value of 0.5 for the CFL number during our simulations to ensure consistency and accuracy.

2. Surface tension terms: the stability condition for the explicit treatment of surface tension is restricted by the appropriate time step resolution of the capillary waves given by [36]:

$$\Delta t_{st} = \sqrt{\frac{\rho_L + \rho_g}{4\pi\sigma}\Delta^3} \tag{7}$$

Equation 7 imposes severe time step restrictions when surface tension is treated explicitly, which was the case in the current research. For example, in case of the liquid monopropellant injection through the pintle injector, based on the properties described in Table 4, for the minimum grid size of 78 μm for the Otto Fuel II injection and atomization case, Δt_{st} is about 38 μs. One way to mitigate it is to use implicit schemes.

3. Viscous terms: the time step restriction imposed by this term is given by:

$$\Delta t_{visc} = \min\left[\frac{\rho(\alpha)_{i,j,k}}{\mu(\alpha)_{i,j,k}}\frac{\Delta^2}{6}\right] \tag{8}$$

The time step chosen for a given instant is given by the minimum of these three times. In our case, Δt_{st} was the limiting time scale.

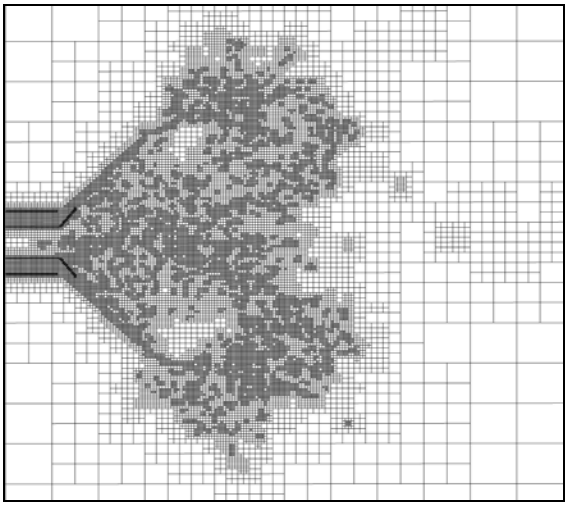

Figure 2. Example of AMR used in this effort.

RESULTS AND DISCUSSION

The results are organized into three sub-sections. The first sub-section presents the numerical challenges encountered during the research effort and our strategy for model validation. This is followed by a section describing our thorough model validation effort using the available experimental data of Petrescu, et al. [16] that used water as the working fluid in pintle injector breakup. Once the model is established, the next sub-section will present a detailed study of breakup and droplet statistics using the physical properties of Otto Fuel II at engine relevant pressures and a discussion on the droplet statistics.

Numerical Challenges and Grid Sensitivity Analysis

Irrespective of the numerical method, the challenges accompanying numerical simulation of incompressible two-phase systems increase dramatically as the density ratio increases [12, 37] The time integration scheme used in the current approach involves a classical time-splitting projection method, which requires the solution of the Poisson equation to obtain the pressure field:

$$\nabla.\left[\frac{\Delta t}{\rho_{n+\frac{1}{2}}}\nabla p_{n+\frac{1}{2}}\right] = \nabla.u_* \tag{9}$$

Equation 9 is solved using a standard multigrid V-cycle methodology, and for large density ratios, its solution suffers from slow convergence rates [38, 39]. One of the ways to overcome this issue is by using extremely high grid resolution, to resolve the steep density gradient and surface tension at the interface and to ensure consistencies in the momentum equation. Another method of speeding up the convergence rate is to spatially filter the interface during reconstruction. Even though the current methodology performs very well for several high-density-ratio systems, including a traveling capillary wave in an air/water system, the convergence of such cases can seriously degrade, depending on the problem and interface topology [13], in comparison with other methods [40]. Atomization phenomena, at large density ratios, is one such configuration. Therefore, in the validation case described in the next section where density ratio is $O(1000)$, we have used both the aforementioned strategies to ensure accuracy: high grid resolution and spatially filtering (at least twice) to ensure numerical accuracy and adequate resolution of the gas-liquid interface.

Model Validation

As a first step, to ensure that the current theoretical framework is capable of accurately resolving the interfacial flow dynamics, we simulate the experiment conducted by Petrescu, et al. [16]. They characterized the spray characteristics in a monopropellant pintle injector, such as the one considered in this study. In these experiments, water is used as the working fluid. The operating conditions consist of chamber pressures of 1 atm and water injection at a rate of 44.4 g/s at room temperature conditions. Table 1 lists the corresponding physical properties. The relevant non-dimensional numbers corresponding to these operating conditions are: $We = \rho_g U^2 d / \sigma = 20$, $Re = 1130$ $\rho_L / \rho_g = 781.25$ and $\mu_L / \mu_g = 52.78$.

Table 1. Physical properties of water and air used for model validation.

physical property	water	air
density (kg/m^3)	1000	1.28
viscosity (Pa·s)	9.5x10^{-4}	1.8x10^{-5}
surface tension (N/m)	0.07275	

Figure 3 shows the schematic of the geometry of the monopropellant pintle injector and the boundary conditions used in this research. Table 2 lists the relevant dimensions that are used in the validation case as they relate to the injector schematic diagram. The minimum grid size is 23 μm with a total maximum grid size of 130 million. The total computational expense was about 67,000 CPU hours. We tried to run the calculation on more than one node, but due to load balancing issues, the best results seemed to be on a single node.

Table 2.Relevant dimensions from the experimental setup in terms of the parameters shown in Figure 3.

d	w	c	θ	ψ	l
4.7 mm	3.9 mm	0.8 mm	80^o	60^o	2d

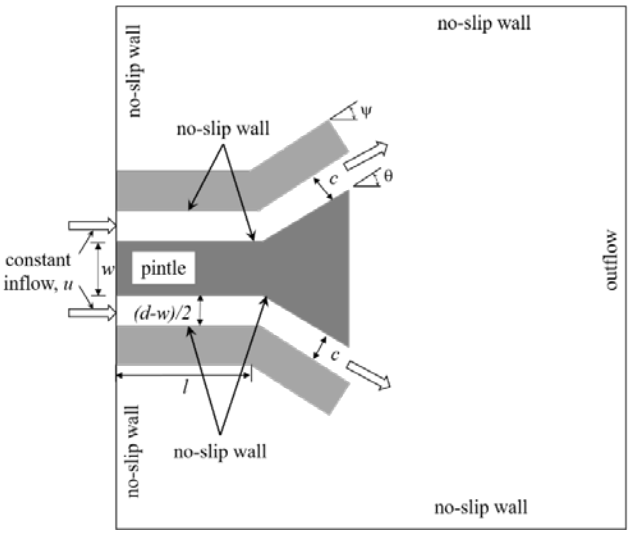

Figure 3. Schematic of the geometry and boundary conditions used in the simulations (figure not to scale).

Figure 4 shows an instantaneous snapshot of the spray showing iso-surface of α, that is, the liquid location. Current model validation consists of the comparison of Sauter mean diameters (SMD) and spray cone angles predicted by the proposed numerical approach against measurements. The measurements were taken at 60, 65, and 70 mm downstream of the injector exit, as shown by the red lines in the figure below. SMD is a statistical measure of the size distribution in a spray and is calculated as follows for each of the three planes:

$$\text{SMD} \equiv D_{32} = \frac{\sum_{i=1}^{\infty} d_i^3}{\sum_{i=1}^{\infty} d_i^2} \qquad (10)$$

Table 3 shows the comparison of our results with measurements of Petrescu, et al. [16] at three downstream locations, showing excellent agreement with a maximum absolute error of 4.04%. Spray angle is also compared with experiments – our results predict an angle of 29.7^o (see figure 4) versus 31^o that is measured in the experiment. The absolute error is 4.2%.

Table 3. Comparison between SMD predicted by the current study vs measurements of Petrescu, et al. [16].

distance from injector (mm)	SMD from experiment (μm) [16]	SMD from present study (μm)	absolute error (%)
60	1291.32	1273.74	1.36
65	1194.56	1242.79	4.04
70	1104.14	1101.92	0.20

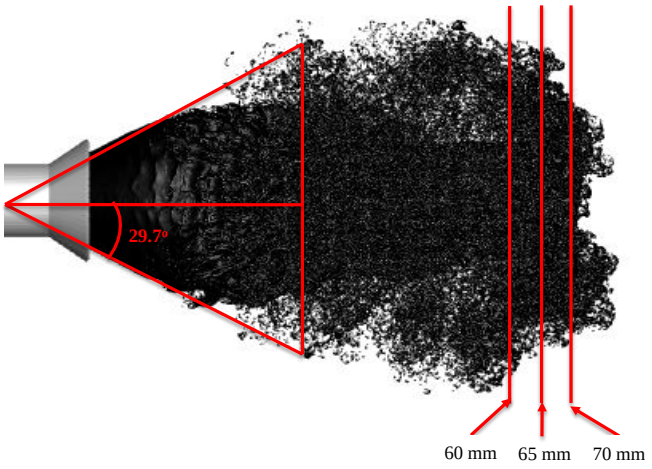

Figure 4. Instantaneous spray field showing iso-surface of the liquid fraction. The experimental measurement locations are identified by the three red lines corresponding to 60, 65 and 70 mm downstream of the injector exit.

Physical processes underlying Otto Fuel II atomization and spray formation

Otto Fuel II is a mixture of 75% 1,2-propylene glycol dinitrate (PGDN), 23% dibutyl sebacate (DBS) and 2% 2-nitrodiphenylamine [41]. Table 4 lists the physical properties of Otto Fuel II relevant to the current research [14, 15]. The operating conditions consists of a chamber pressure, p = 106.2 bar, temperature, T = 300 K, and inlet velocity u = 3.34 m/s, corresponding to a density ratio of 10, dynamic viscosity ratio of 212, liquid-based Reynolds number of 748 and Weber number of 20 (based on gas density). The geometry that is used to investigate the spray and atomization characteristics of this monopropellant is the same as was used for the validation case. It should be noted that Otto Fuel II is 4.6 times as viscous as water.

Table 4. Physical properties of Otto Fuel II.

physical property	Otto Fuel II	air
density (kg/m^3)	1232	123.2
viscosity (Pa·s)	4.4x10^{-3}	1.8x10^{-5}
surface tension (N/m)	0.03445	

Since no experimental data is available for Otto Fuel II at the conditions of interest, to ensure accuracy, grid sensitivity studies were conducted. Figure 5 shows the evolution of liquid fuel from the pintle injector using grid levels of 8 and 9. As can be inferred from the time evolution images, the global behaviors of the cone angle and the cone formation are similar. Thus level 8 was used to conduct the complete analysis of this case. It should be noted that breakup (pinch-off) occurs at molecular scales, so as the grid resolution is increased, one should expect the details to change, however, the global behaviors such as the cone angle converge to a reasonably stable value.

Figure 6 shows the time evolution of the series of events that follow as Otto Fuel II is injected in a quiescent chamber. Figure 7 shows the corresponding grid as it adapts to resolve the relevant flow physics. In this case, the minimum grid size is 46 µm with a total of 28.6 million and a total computational expense of 45,000 CPU hours. Two grid adaptation criteria are used – (1) based on the gradient of the volume of fraction variable, α to capture the liquid-gas interface, and (2) value-based refinement to refine the liquid interior. It should be noted that simulations with AMR utilize less than 1% of the grid points in comparison to uniform grid size studies with 46 µm, thus making this calculation possible. One of the major difference between this case and the validation case is the density ratio (10 in this case as compared to 781 for the validation case), which resulted in over an order of magnitude in the number of grid points for the validation case, not only because a higher grid-level was used in that case to appropriately resolve the liquid/gas interface, but also since water is 4.6 times less viscous than Otto Fuel II, resulting in more intense atomization and production of an order of magnitude more number of droplet production.

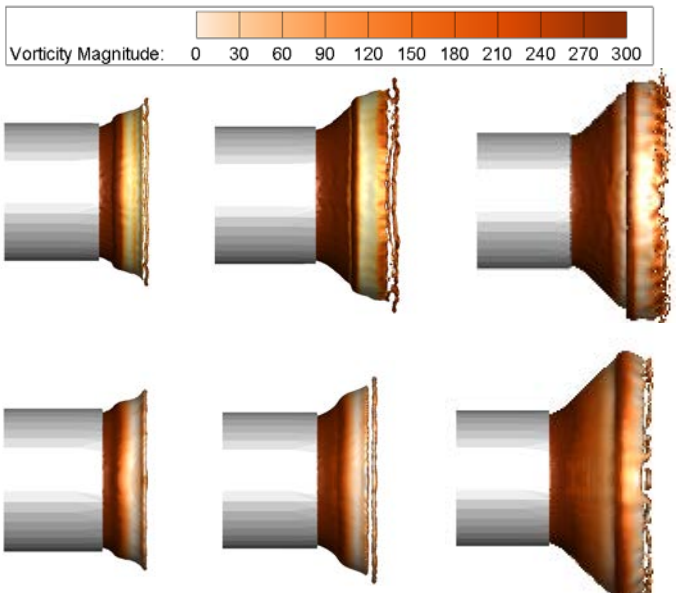

Figure 5. Grid sensitivity analysis, level 9 results in the top row and level 8 on the bottom. The liquid interface is colored by the vorticity magnitude. The cone angles and the general development are close to each other.

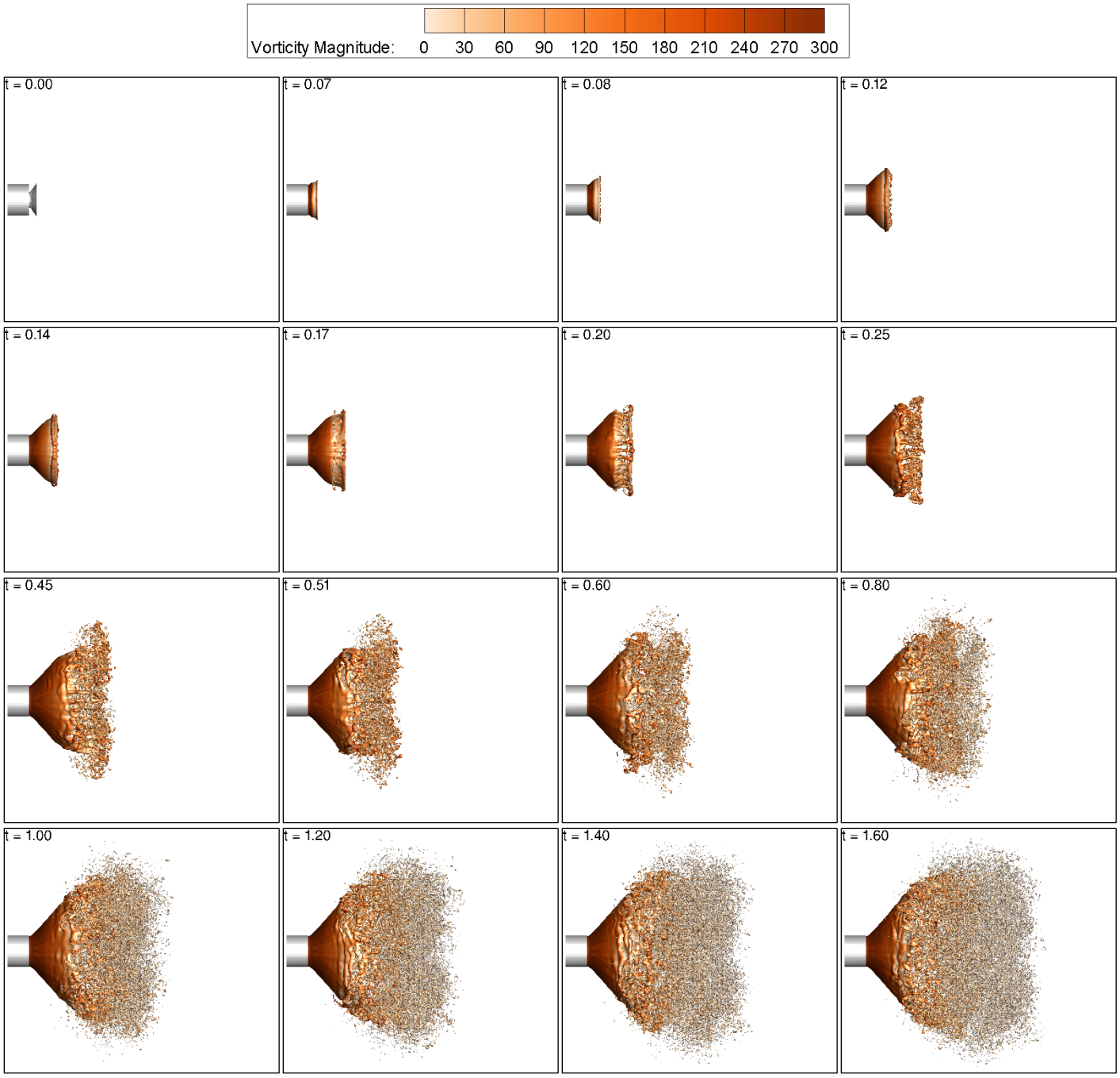

Figure 6. Time evolution of Otto Fuel II spray as it is injected from a pintle injector. The figures show iso-contours of the liquid fraction and the colors indicate vorticity magnitude. Non-dimensional time, t = T/(u/d).

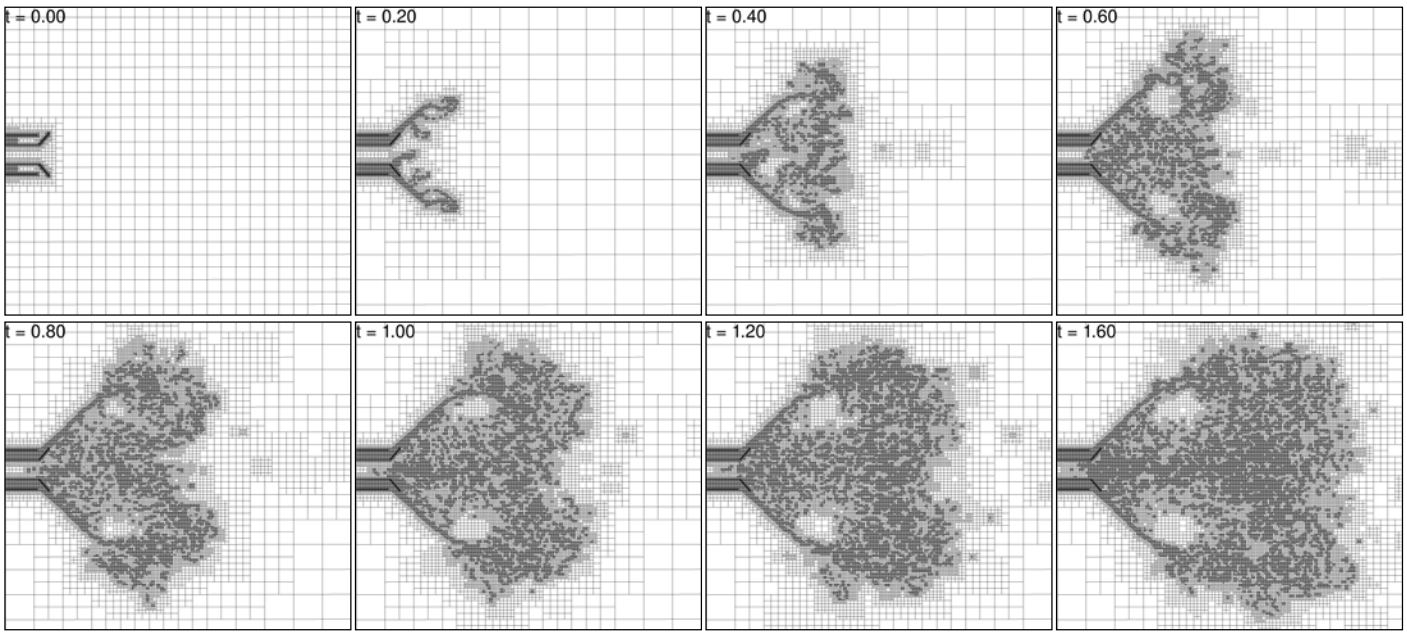

Figure 7. Time evolution as grid adapts to resolve the liquid-gas interface and the liquid interior. Non-dimensional time, t = T/(u/d).

As observed in figures 6 and 7, the viscous liquid emanates from the injector exit, the liquid spreads radially and forms a hollow cone that consists of a rim at the edge of the cone. The mechanisms that lead to spray formation can be explained in three major steps: first, aerodynamic drag acts on the liquid cone as the cone penetrates the chamber that leads to the detachment of the rim as seen in figure 8 at the non-dimensional time, t = 0.08 (see zoomed-in image in figure 8 on the left). Second, as the cone further develops, in addition to the rim, a lip is formed that is curled in the outward direction as seen at times corresponding to t = 0.12-0.20 (see image on the right in Figure 8). Third, the thickness of the rim continues to grow then stretches, detaches from the lip and breaks up into ligaments and droplets. Simultaneously, as the rim detaches, the lip retracts due to surface tension and forms another rim. These processes are shown at t = 0.25. It should be noted that the higher viscosity of the liquid (as compared to the validation case that used water), causes the stretching of the lip, a phenomenon not observed for water (not shown here). The ligament and droplets produced from the breakup of the rim have substantially lower velocities as compared to the evolving cone, and as a result, the radially expanding cone encompasses these structures. This mechanism is further sustained by the two symmetric recirculation zone in the interior of the hollow cone, as shown in figure 9. These primary atomization structures interact with the hollow cone and lead to the formation of instability waves that are seen more prominently for t > 1.00 (see figure 6). The three processes, that is, rim and lip formation, stretching of lip and detachment of the rim due to amplification of instabilities, and the subsequent interaction between the ligaments and droplets produced from rim breakup and the hollow cone serve to further initiate instabilities, continues to form a dense spray. As the spray expands, further axial movement of the cone is hindered because of the low-pressure recirculation zones in the interior of the hollow cone. This leads to the coalescence of droplets and ligaments, thus increasing the effective droplet sizes that are trapped in the low-pressure region while reducing the growth rate of the number of droplets in the chamber. This will be discussed further in the next section that focuses on droplet statistics resulting from this atomization process.

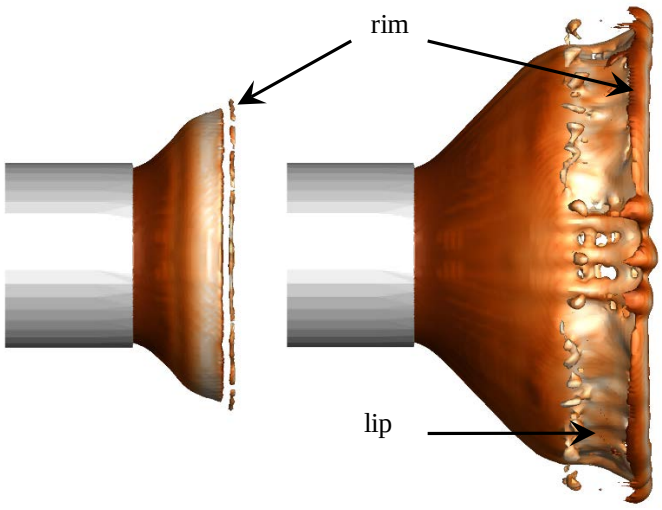

Figure 8. Zoomed in picture showing the formation of the lip, its extension, and the rim.

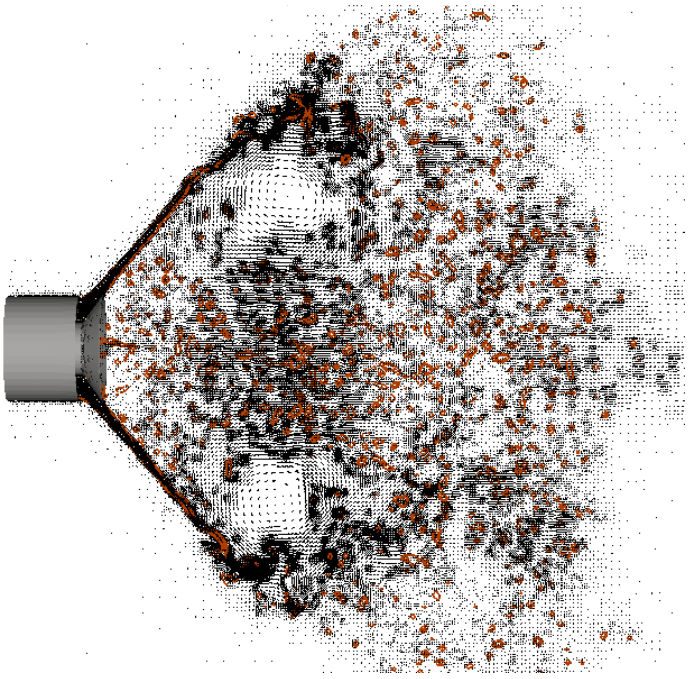

Figure 9. Center plane of the spray showing the hollow cone (orange color) and the recirculation zones represented by velocity vectors at t = 1.2.

Droplet Statistics

Figure 10a shows the time evolution of the droplet production. For non-spherical droplets and ligaments, an effective spherical diameter is calculated based on the volume of the liquid structure. A distinct reduction in the production rate is observed at non-dimensional time of 0.9. This observation can be correlated with the atomization physics – the change in the slope of the droplet production coincides with the strength of the recirculation zone that leads to significant droplet coalescence, thus, even though the mass flow rate of the fuel through the injector is constant, the rate of increase in the number of droplets reduces. The number probability of the droplet sizes is shown in Figure 10b. The most probable size is 150 µm. It should be noted that the droplet sizes only include the liquid structures that result from at least one breakup, thus, the intact liquid sheet in the hollow cone is removed when the droplet sizes are calculated. If we compare the distribution obtained from our calculation with that of a log-normal fit, it is seen that the log-normal distribution is a little broader as compared to current simulations, with the most probable size at about 190 µm.

The large-sized droplets, which contain most of the mass form the tail of the number based probability distribution. Therefore, we analyze the time evolution of Sauter mean diameter (SMD) distribution of the spray using the definition previously used in the validation case and described by equation 10. Figure 11 shows how SMD changes as the atomization of the fuel injected through the pintle injector proceeds in the chamber. After the initial transients, SMD stabilizes at t = 0.9, which also coincides with the change in the slope of the rate of droplet production.

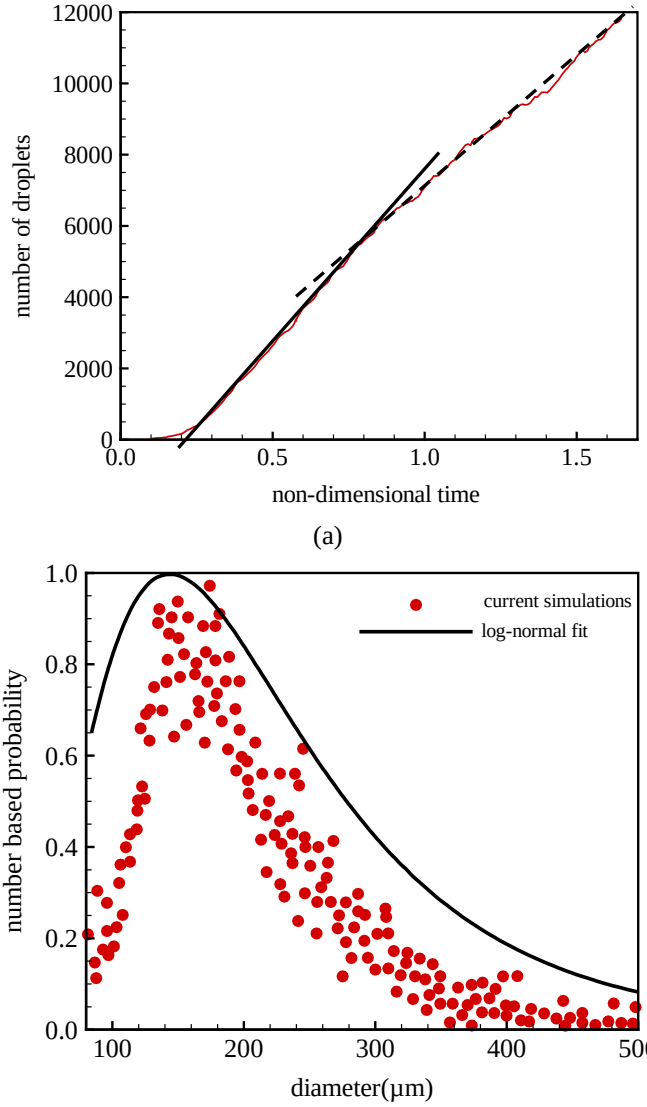

Figure 10. (a) Number of droplets produced as a function of time; and (b) droplet size distribution (non-spherical droplets and ligaments, an effective spherical diameter is calculated based on the volume of the liquid structure)

Finally, the spray dynamics and evolution of the two cases, that is, the validation case with water injection at a chamber pressure of 1 bar and the Otto Fuel II injection case at a chamber pressure of 106 bar at the same flow rate (that leads to different inlet velocities and consequently different Reynolds and Weber numbers), are compared. Phenomenologically, we expect the spray angle to be larger for the high-pressure case because of the increased drag resulting from higher-density gas. This data was extracted from the two simulations confirming our hypothesis, as shown in figure 12. It should be noted that, even though the

flow rates are similar, these two cases are considerably different from each other because of the operating conditions and physical properties of the two liquids, so a direct quantitative comparison is not of much significance.

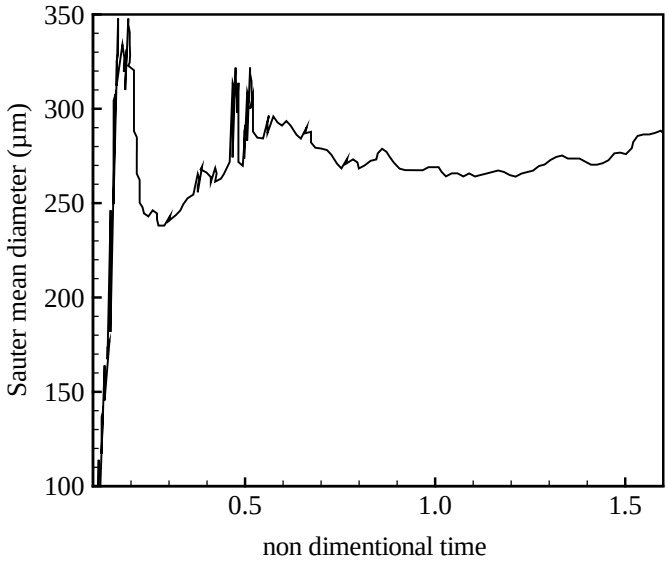

Figure 11. Time evolution of Sauter mean diameter.

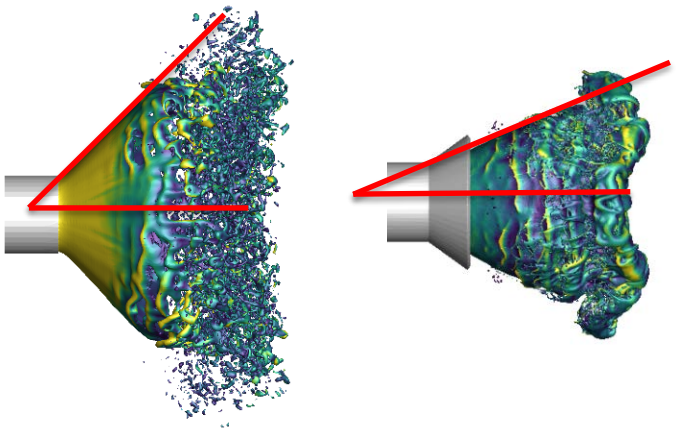

Figure 12. Cone angles of the Otto Fuel II injection (left, about 47°) and water injection (right, 29°) cases. The liquid surface is colored by the vorticity magnitude.

CONCLUSIONS AND FUTURE WORK

In this research, the fundamental processes that lead to the breakup and spray formation when a viscous fuel, Otto Fuel II, injected through a pintle injector ware investigated. It was found that the atomization physics proceeds in three steps – (1) the initial detachment of the rim; (2) the formation, stretching, detachment and atomization of the lip and a thicker rim; and (3) the interaction of the ligaments and droplets produced from rim breakup with the hollow cone that further amplifies the instabilities that cause the rim formation and breakup. This process recursively takes place and leads to the formation of a dense spray. A strong low-pressure recirculation zone is formed in the hollow cone that consumes products of rim atomization and prevents further expansion of the cone, both in radial and axial directions. Droplet size distribution, both based on number-based probabilities and mass-based, Sauter mean diameters are also analyzed in the current effort. Because of the formation of a strong recirculation zone, the growth rate of the number of droplets reduces due to droplet collision and coalescence. These simulations provide unique insights into the underlying breakup mechanism in the dense region where experiments remain limited, and therefore the results are vital for spray model development.

Future work will be focused on identifying the mechanisms underlying the atomization process during throttling. This will be followed by detailed investigations of vaporizing and reacting Otto Fuel II as it is injected in the chamber through the pintle injector.

ACKNOWLEDGEMENTS

This research was supported by the Ohio Space Grant Consortium (OSGC). The authors would like to acknowledge the Advanced Research Computing (ARC) center at the University of Cincinnati for the computational infrastructure. The authors also thank Dr. Stephane Pópinet for allowing them to use his VOF and AMR algorithms.

REFERENCES

[1] Faeth, G. M., "Dynamics of secondary drop breakup—a rate controlling process in dense sprays," Proc. ILASS-Europe.
[2] Berthoumieu, P., Carentz, H., Villedieu, P., and Lavergne, G., 1999, "Contribution to droplet breakup analysis," International Journal of Heat and Fluid Flow, 20, pp. 492-498.
[3] Dressler, G., and Bauer, J., 2000, "Trw pintle engine heritage and performance characteristics," 36th aiaa/asme/sae/asee joint propulsion conference and exhibit, American Institute of Aeronautics and Astronautics.
[4] Casiano, M. J., Hulka, J. R., and Yang, V., 2010, "Liquid-propellant rocket engine throttling: A comprehensive review," Journal of Propulsion and Power, 26(5), pp. 897-923.
[5] Sakaki, K., Kakudo, H., Nakaya, S., Tsue, M., Kanai, R., Suzuki, K., Inagawa, T., and Hiraiwa, T., 2016, "Performance evaluation of rocket engine combustors using ethanol/liquid oxygen pintle injector," 52nd AIAA/SAE/ASEE Joint Propulsion Conference.
[6] Son, M., Yu, K., Radhakrishnan, K., Shin, B., and Koo, J., 2016, "Verification on spray simulation of a pintle injector for liquid rocket engine," Journal of Thermal Science, 25(1), pp. 90-96.
[7] Nardi, R., Perez, V., and Pimenta, A., 2015, "Experiments with pintle injector design and development," 51st AIAA/SAE/ASEE Joint Propulsion Conference.
[8] Bravo, L., Kim, D., Ham, F., Powell, C., and Kastengren, A., 2019, "Effects of fuel viscosity on the primary breakup dynamics

of a high-speed liquid jet with comparison to x-ray radiography," Proceedings of the Combustion Institute, 37(3), pp. 3245-3253.
[9] Bravo, L., Kim, D., Ham, F., and Su, S., 2018, "Computational study of atomization and fuel drop size distributions in high-speed primary breakup," 28(4), pp. 321-344.
[10] Owkes, M., and Desjardins, O., 2014, "A computational framework for conservative, three-dimensional, unsplit, geometric transport with application to the volume-of-fluid (vof) method," Journal of Computational Physics, 270, pp. 587-612.
[11] Wang, S., and Desjardins, O., 2018, "3d numerical study of large-scale two-phase flows with contact lines and application to drop detachment from a horizontal fiber," International Journal of Multiphase Flow, 101, pp. 35-46.
[12] Gorokhovski, M. a. H. M., 2008, "Modeling primary atomization," Annual Review of Fluid Mechanics, 40(1), pp. 343--366.
[13] Pópinet, S., 2009, "An accurate adaptive solver for surface-tension-driven interfacial flows," Journal of Computational Physics, 228, pp. 5838-5866.
[14] Gaworski, C., Leahy, H., Bashe, W., Macewen, J., Vernot, E., and Haun, C., 1985, "A one-year inhalation toxicity study of otto fuel 2," University of California, AAMRL-TR-85-071
[15] Abadin, H., and Llados, F., 1995, "Toxicological profile for otto fuel ii and its components," Department of Health and Human Services, Agency for Toxic Substances and Disease Registry, Atlanta, GA.
[16] Petrescu, V., Schrijer, F., and Zandbergen, B., 2017, "Atomized spray properties in pintle injection," TU Delft, https://vladpetrescu.files.wordpress.com/2017/10/atomization_research.pdf.
[17] Khare, P., 2014, "Breakup of liquid droplets," Ph.D., Ph.D. Thesis Georgia Institute of Technology.
[18] Almgren, A., Bell, J., and Crutchfield, W., 2000, "Approximate projection methods: Part i. Inviscid analysis," SIAM Journal on Scientific Computing, 22(4), pp. 1139-1159.
[19] Scardovelli, R., and Zaleski, S., 1999, "Direct numerical simulation of free-surface and interfacial flow," Annual Review of Fluid Mechanics, 31(1), pp. 567-603.
[20] Popinet, S., 2003, "Gerris: A tree-based adaptive solver for the incompressible euler equations in complex geometries," J Comput Phys, 190(2), pp. 572-600.
[21] Khare, P., 2014, "Breakup of liquid droplets," Ph.D., Georgia Institute of Technology.
[22] Zakerzadeh, S. A., 2008, "Applying dynamic contact angles to a three-dimensional vof model," PhD, University of Toronto.
[23] Bergmans, J., Keppens, R., Odyck, D. E. A., and Achterberg, A., 2005, "Simulations of relativistic astrophysical flows," Adaptive mesh refinement - theory and applications, T. Plewa, T. Linde, and V. Gregory Weirs, eds., Springer Berlin Heidelberg, pp. 223-233.
[24] Bryan, G., and Norman, M., 2000, "A hybrid amr application for cosmology and astrophysics," Structured adaptive mesh refinement (samr) grid methods, S. Baden, N. Chrisochoides, D. Gannon, and M. Norman, eds., Springer New York, pp. 165-170.
[25] Choptuik, M., 2000, "Making arbitrarily small black holes: Experiences with amr in numerical relativity," Structured adaptive mesh refinement (samr) grid methods, S. Baden, N. Chrisochoides, D. Gannon, and M. Norman, eds., Springer New York, pp. 153-163.
[26] Bell, J., 2005, "Amr for low mach number reacting flow," Adaptive mesh refinement - theory and applications, T. Plewa, T. Linde, and V. Gregory Weirs, eds., Springer Berlin Heidelberg, pp. 203-221.
[27] Jourdren, H., 2005, "Hera: A hydrodynamic amr platform for multi-physics simulations," Adaptive mesh refinement - theory and applications, T. Plewa, T. Linde, and V. Gregory Weirs, eds., Springer Berlin Heidelberg, pp. 283-294.
[28] Myers, C., 2000, "The dynamics of localized coherent structures and the role of adaptive software in multiscale modeling," Structured adaptive mesh refinement (samr) grid methods, S. Baden, N. Chrisochoides, D. Gannon, and M. Norman, eds., Springer New York, pp. 111-125.
[29] Pernice, M., Bockelie, M. J., Swensen, D., and Smith, P. J., 2000, "Progress, results, and experiences in developing an adaptive solver for steady state turbulent reacting flows in industrial boilers and furnaces," Structured adaptive mesh refinement (samr) grid methods, S. Baden, N. Chrisochoides, D. Gannon, and M. Norman, eds., Springer New York, pp. 127-151.
[30] Chen, X., Ma, D., Khare, P., and Yang, V., 2011, "Energy and mass transfer during binary droplet collision," 49th AIAA Aerospace Sciences Meeting including the New Horizons Forum and Aerospace Exposition, AIAA 2011-771.
[31] Notaro, V., Khare, P., and Lee, J. G., 2018, "Mixing characteristics of non-newtonian impinging jets at elevated pressures," Flow, Turbulence and Combustion, https://doi.org/10.1007/s10494-018-9955-x.
[32] Windland, K., and Khare, P., 2017, "The effect of inlet pulsations on liquid jet atomization," ASME Dayton Engineering Sciences Symposium.
[33] Ma, D.-J., Chen, X.-D., Khare, P., and Yang, V., 2011, "Atomization patterns and breakup characteristics of liquid sheets formed by two impinging jets," AIAA Paper, 2011-97, pp. 2011-2097.
[34] Khare, P., Ma, D., Chen, X., and Yang, V., 2012, "Phenomenology of secondary breakup of newtonian liquid droplets," 50th AIAA Aerospace Sciences Meeting including the New Horizons Forum and Aerospace Exposition, AIAA-2012-0171.
[35] Gamertsfelder, J., and Khare, P., 2018, "Injector dynamics and atomization behaviors of liquid monopropellants in pintle injectors," ASME 14th Dayton Engineering Sciences Symposium, DESS2018-030.
[36] Brackbill, J. U., Kothe, D. B., and Zemach, C., 1992, "A continuum method for modeling surface tension," Journal of Computational Physics, 100, pp. 335-354.
[37] Desjardins, O., and Moureau, V., 2010, "Methods for multiphase flows with high density ratio," Center for Turbulence Research (CTR).
[38] Alcouffe, R., Brandt, A., Dendy, J., J., and Painter, J., 1981, "The multi-grid method for the diffusion equation with strongly

discontinuous coefficients," SIAM Journal on Scientific and Statistical Computing, 2(4), pp. 430-454.
[39] Chan, T. F., and Wan, W. L., 2000, "Robust multigrid methods for nonsmooth coefficient elliptic linear systems," Journal of Computational and Applied Mathematics, 123(1–2), pp. 323-352.
[40] Gerlach, D., Tomar, G., Biswas, G., and Durst, F., 2006, "Comparison of volume-of-fluid methods for surface tension-dominant two-phase flows," International Journal of Heat and Mass Transfer, 49(3–4), pp. 740-754.
[41] NRC, 2002, Acute exposure guideline levels for selected airborne chemicals: Volume 2, The National Academies Press, Washington, DC.